

# An Investigation on the Adsorption Behavior of a Mesoporous Silica Synthesized by a Surfactant-Assisted Method in an Acidic Media

F. Salehtash, H. Banna Motejadded Emrooz and M. Jalaly\*

\* maisam\_jalaly@iust.ac.ir

Received: September 2017 Accepted: January 2018

Nanotechnology Department, School of New Technologies, Iran University of Science & Technology, Tehran, Iran.  
DOI: 10.22068/ijmse.15.2.48

**Abstract:** Mesoporous SiO<sub>2</sub> nanopowder was synthesized under an acidic condition through a sol-gel method by use of cetyltrimethyl ammonium bromide (CTAB) as the structure directing agent. Also, the effects of the surfactant content (0, 0.5, and 1 g) were examined. The samples were investigated using the XRD, SEM, FTIR, TEM and N<sub>2</sub> adsorption-desorption analyses. The results revealed that the sample containing 1 g CTAB surfactant had the highest specific surface area of ~ 549 m<sup>2</sup>.g<sup>-1</sup>, and showed the lowest values of 4.1 nm and 0.56 cm<sup>3</sup>.g<sup>-1</sup> for pore size and pore volume, respectively. Adsorption behavior of the mesoporous silica was investigated for the degradation of methylene blue pigments (MB) in aqueous solutions. The samples containing 0, 0.5 and 1 g CTAB exhibited the maximum adsorption capacities of 333, 454 and 526 mg/g, respectively.

**Keywords:** Mesoporous silica, Sol-gel, Adsorption, Methylene blue.

## 1. INTRODUCTION

It was Mobil Corporation, which for the first time in 1992 developed a new class of materials having unique mesoporous structures (pore diameter ranging from 2 to 50 nm). This achievement was a platform for further developments of many new types of molecular sieves and porous materials [1, 2]. SiO<sub>2</sub> is one of the most attractive oxides which can be produced in the mesoporous form. This porous structure may be used in extensive areas such as catalysts, biomaterials, biosensors, biological targets, drug delivery systems, implants, chromatographic supports for biomolecule purification and analysis, and adsorbents for toxic substances and pollutants [3– 6]. The outstanding advantages of this mesoporous oxide include high surface area, ordered pores, high volume of pores and consequently high adsorption capacity, narrow pore size distribution, non-toxicity, and high biocompatibility. Among mesoporous materials, silicon oxide has been of particular interest for researchers due to its high potential for achieving an ordered mesoporous structure [7].

CTAB is one of the best cationic surfactants which is frequently utilized in the laboratory and industry. CTAB is composed of a polar head and a non-polar chain [8]. The length of alkyl chain of

this surfactant may vary. The longer the alkyl chain, the greater the density of the micelle's surface charge; as a result, the surface of the micelle acts as a catalyst and speeds up the rate of the particle formation [9]. Various parameters including solvent type (water or alcohol) and the ratio of water to alcohol can affect the micellization [10]. Lee et al. studied the synthesis of mesoporous silica by use of styrene sulfonate or sodium dodecyl sulfate as etchants, and examined the removal of toxic organic pollutants [11].

Artificial dyes are a group of organic contaminants, widely used in weaving, paper-making, printing, leather, tannery, cosmetics, plastics and nutrition industries. There are several types of commercial dyes, which owing to the instability of the dye molecules on the fabric along with inefficiency of dyeing, a considerable fraction of these dyes enter the industrial wastewater. Sewage from textile weaving and dyeing industries are one of the most problematic issues in terms of wastewater as they contain chemicals, suspended materials, poisonous compounds, and pigments (the first pollutants that can be detected by human eyes). Dyes might significantly decrease light penetration, thus influencing the light-based activities of aquatic lives, the appearance of eutrophication

phenomenon, presence of suspended materials, and turbidity of the water. Therefore, dye removal from a wastewater is essential and inevitable. Methylene blue (MB) is an aromatic chemical dye, which has a useful and important role in the textile industry. Since it is aromatic and often toxic, this dye may be carcinogen, mutagenic, and resistant to biological decomposition. Photocatalytic oxidation process by ultraviolet (UV) light in the presence of catalysts such as titanium dioxide, zirconium dioxide, zinc oxide, and silicon oxide for elimination of organic pollutants, is a kind of advanced oxidation processes, which has received significant attention due to its high efficiency [12–18]. Nowadays, silicon oxide is being used for removal of a widespread range of organic compounds because of its stability against light and chemical corrosion, nontoxicity, and ability to adsorb a wide spectrum of the electromagnetic waves [20–22].

Synthesis procedure of ordered mesoporous silica is a well-known protocol and widely used in different investigations. To the best of our knowledge, mesoporous silica has been regularly synthesized in basic conditions using tetraethyl orthosilicate (TEOS) precursor. Herein, we introduced another protocol for the material synthesis in the sol-gel route. Also, it was attempted to evaluate the influence of the synthesized mesoporous silica as an affordable adsorbent to remove MB contamination from aqueous environments. Various parameters such as the CTAB amount, contact time, and primary dye concentration were examined.

## 2. EXPERIMENTAL

### 2. 1. Materials

Tetraethyl orthosilicate (TEOS) as silica precursor and 65% nitric acid as catalyst were purchased from the Merck Millipore Co. (Germany). CTAB as the structure directing agent and cationic methylene blue were also purchased from the Daejung Co. (South Korea) and Mojallali Co. (Iran), respectively. Deionized water was also used as a solvent.

### 2. 2. Synthesis Procedure

First, deionized water and TEOS were mixed together using a magnetic stirrer. The desired amount of CTAB was then added and the solution was slowly stirred to obtain a fully colorless mixture. After that, nitric acid was added dropwise so that the pH of the solution was adjusted to 1, and the final mixture was stirred at a rotating speed of 500 rpm for 30 minutes to prepare a silica sol. In each experiment, the volumes of the materials used (TEOS, H<sub>2</sub>O, and HNO<sub>3</sub>) were 16, 20, and 15 ml, respectively. The amount of CTAB (x) was considered to be 0, 0.5, and 1 g in order to investigate the effect of CTAB content (the samples were nominated as SC0, SC0.5, and SC1, respectively). The prepared sol was heated in a Teflon-lined stainless steel autoclave for 4 h at 160 °C. Subsequently, the precipitated gel washed several times by deionized water for sake of purification and then, it was filtered and dried at 80 °C. Afterwards, the dried material was calcined in an electric furnace (Azar Furnace Co., TF5/40-1500) at 700 °C for 5 h at an incremental rate of 10 °C/min.

### 2. 3. Characterization

Thermal behavior of the non-calcined powder was studied by differential thermal analysis (DTA) and thermal gravimetry (TG) in a STA-504 Bähr simultaneous thermal analyzer (STA) using a constant heating rate of 10 °C/min from 25 to 900 °C. DTA measurements were accomplished under an argon atmosphere. The adsorption behavior of the synthesized samples was investigated. The adsorption time was studied for a 100 ppm MB aqueous solution. Also, the adsorption capacities of the synthesized products were evaluated using MB solutions with various initial concentrations of 50, 100, 200, 400, 800 and 1000 ppm. In these experiments, the final, equilibrium concentrations of MB after 20 min exposure of silica to the MB solutions of the different initial concentrations were determined. The volume of MB-contaminated solutions were fixed to be 10 ml, and the adsorption experiments were conducted under stirring with a rate of 800 rpm. Once the pigment completely adsorbed,

UV-vis spectroscopy (UV-1200, Reyleigh) was performed in a range of 400 to 700 nm on the remaining solution in order to acquire quantitative and qualitative analyses about adsorption of the dye. The adsorption capacity was quantified using the following formula:

$$Q_e = \frac{(C_0 - C_e) V}{m} \quad (1)$$

$$Q_e = \frac{Q_m b C_e}{1 + b C_e} \quad (2)$$

where  $Q_e$  and  $Q_m$  (mg/g) are the equilibrium and maximum adsorption capacities, respectively,  $m$  (mg) is the adsorbent mass,  $C_0$  (mg/l) is the initial concentration of MB,  $C_e$  is the equilibrium concentration (mg/l),  $b$  is the equilibrium constant (l/mg), and  $V$  (l) is the volume of solution [24, 25].

To determine the phases, the XRD analysis of the samples calcined at 700 °C were checked by a PW1800-XRD Philips. In addition, low-angle X-ray diffractometer was used in order to study the effect of the CTAB amount on the order of pores. To examine the morphology of the powder, scanning electron microscope (SEM, TESCAN VEGA/XTM TESCAN) and transmission electron microscope (TEM, CM120, Philips) were used. Fourier-transform infrared (FTIR) spectroscopy (Perkin Elmer) was performed on the specimens before and after calcination treatment in order to analyze the existing groups on the surface as well as the level of surfactant removal. The porous structures of the samples were investigated using nitrogen adsorption-desorption isotherms (BET) at 77 K. Prior to conducting BET analysis, samples were degassed for 5 h at 150 °C.

### 3. Results and Discussion

To obtain the required temperature for the calcination treatment, a dried, non-calcined sample prepared by sol-gel process was subjected to the thermal analysis. Fig. 1 shows the result of thermal analysis of the sample SC1 before calcination. As the temperature increased up to

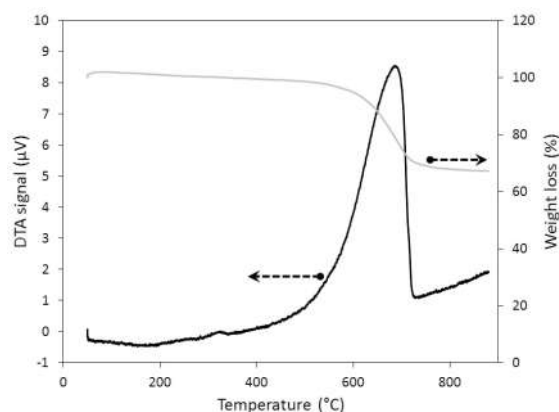


Fig. 1. Thermal analysis of SC1 sample before calcination.

650 °C, a great exothermic peak appears which may be assigned to the oxidation of different organic groups in the sample. This exothermic reaction is accompanied with a great weight loss (~30%), confirming the elimination of organic groups during heat treatment. The weight loss curve is in a good agreement with DTA curve. It is clear that the conversion process occurred completely after this exothermic signal, and hence, the value of 700 °C was selected for the calcination temperature.

Fig. 2 (a) shows the XRD pattern of the mesoporous silica synthesized using 1 g CTAB additive (SC1 sample). As depicted in this figure, amorphous nature of the material is clearly observed. To check the mesoporous structure of our silica, low angle XRD analysis was performed on the same sample (Fig. 2 (b)). As can be observed in this pattern, there is a clear peak located at approximately 1.5°, which is related to (100) plane of the porosity network [26]. For highly ordered mesoporous structures, at least two other small peaks are usually observed below 6° [27]. The absence of such peaks in our low-angle pattern may suggest that there is no complete long-range order in the mesophases of our samples. The probable reaction between negative ions (cetyltrimethyl ammonium obtained from CTAB ionization) and positive ions (H<sup>+</sup> obtained from nitric acid ionization) in acidic media may be the reason for the non-appearance of a highly-ordered

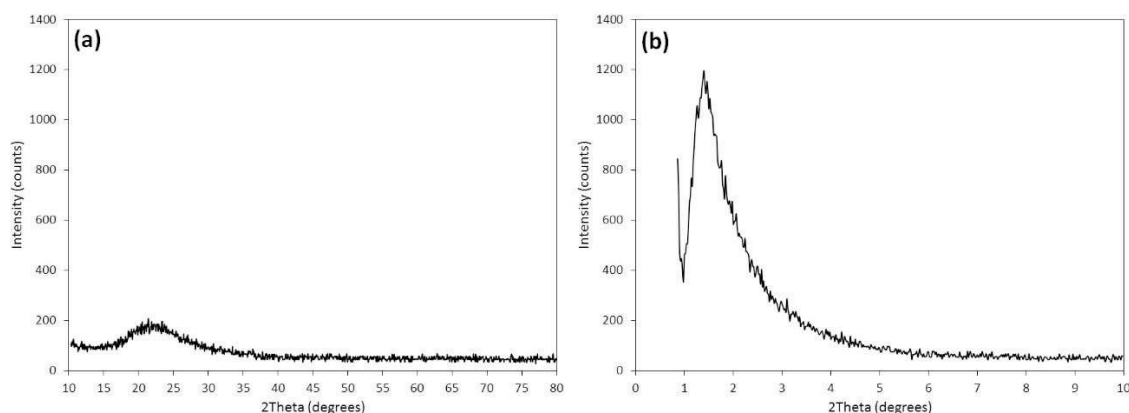


Fig. 2. (a) Normal XRD and (b) low-angle XRD patterns for mesoporous SC1 sample.

mesoporous structure.

SEM micrograph of the synthesized sample SC1 is depicted in Fig. 3 (a). According to this image, nanometric clusters of 50–70 nm in diameter were formed which were composed of nanoparticles. Furthermore, the agglomeration of the particles and clusters can be clearly observed in this sample, which occurs due to the tendency of particles towards reducing surface energy. Fig. 3 (b) illustrates a cluster of nanoparticles of SC1 sample in a typical TEM micrograph. As can be

seen, SiO<sub>2</sub> nanoparticles formed during the sol-gel method had an average diameter of ~5 nm. The porous structure of the sample containing nearly spherical SiO<sub>2</sub> particles are clearly observed in these images. The morphology of porous particles were wormlike, among which a high level of order was not observed in the structure, confirming the low-angle XRD result.

Nitrogen adsorption-desorption curves and also the pore distributions of all synthesized samples are demonstrated in Fig. 4 (a) and (b). In

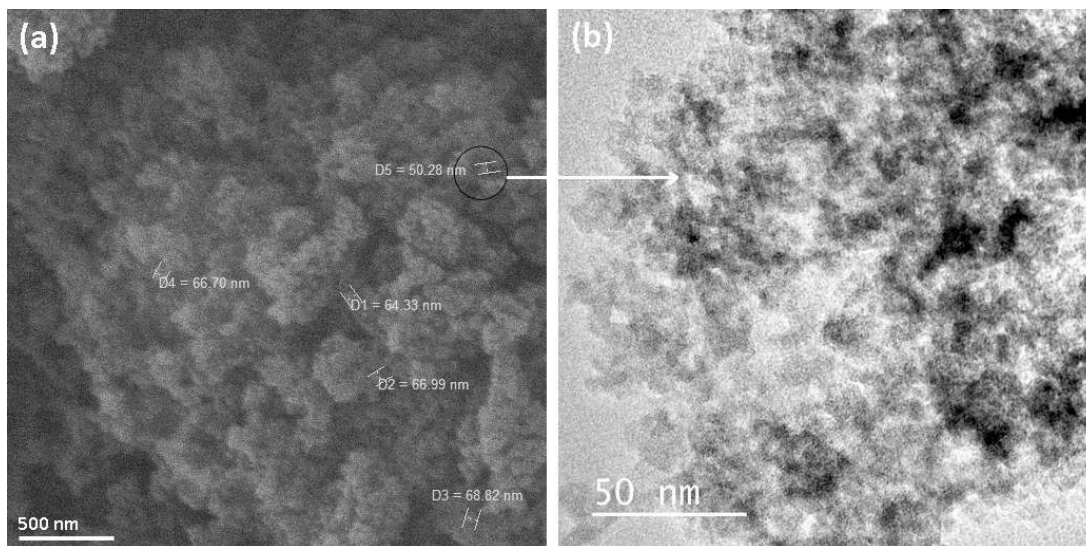


Fig. 3. SEM (a) and TEM (b) micrographs of the synthesized SC1 sample after calcination.

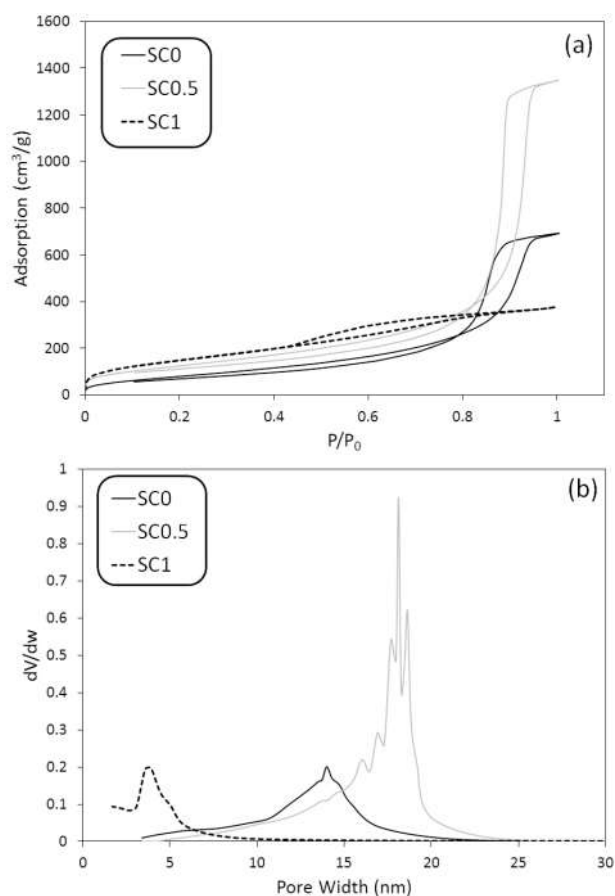


Fig. 4. (a) Nitrogen adsorptions–desorption isotherms and (b) pore size distribution, of SC0, SC0.5 and SC1 samples.

case of BET curves of SC0 and SC0.5 samples, an abrupt increase in adsorption was observed at the relative pressure of  $\sim 0.8$ , while SC1 sample shows a relatively moderate increase in nitrogen adsorption. In fact, after its initial increase, a smooth rise in the adsorption curve of this sample is obvious. The lowest adsorption level for SC1 sample is an indicator that this sample has the smallest pore size which is consistent with Fig. 4 (b). BET surface areas, average pore sizes, as well as total pore volumes of the synthesized samples are tabulated in Table 1. It can be seen that an increase in the surfactant amount resulted in an increase in the surface area from 314.7 to 548.8  $\text{m}^2\cdot\text{g}^{-1}$ . Also by increasing CTAB content, the (diameter/volume) of the pores increased from  $\sim (13 \text{ nm}/1 \text{ cm}^3\cdot\text{g}^{-1})$  to  $\sim (17 \text{ nm}/2 \text{ cm}^3\cdot\text{g}^{-1})$ , followed by a decrease to  $\sim (4 \text{ nm}/0.5 \text{ cm}^3\cdot\text{g}^{-1})$ .

The reduction of pore volume in SC1 sample is the result of smaller pore size of this sample compared to the other samples which is clear in Fig. 4 (b). Regarding BET curves, all samples show type IV standard curves with capillary condensation steps which signify the presence of mesopores. The effect of CTAB content on the surface area of the synthesized nanoparticles are consistent with Hilogna et al.'s findings [28].

Table 1. Features of silica nanoparticles based on N<sub>2</sub> adsorption-desorption test.

Sample	BET surface area ( $\text{m}^2\cdot\text{g}^{-1}$ )	Average pore size (nm)	Total pore volume ( $\text{cm}^3\cdot\text{g}^{-1}$ )
SC0	314.7	13.1	1.03
SC0.5	468.3	17.3	2.02
SC1	548.8	4.1	0.56

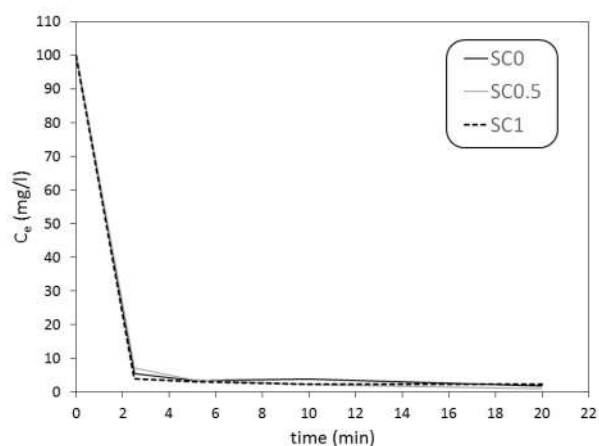


Fig. 5. The efficiencies of the synthesized mesoporous silica for MB removal from aqueous solution.

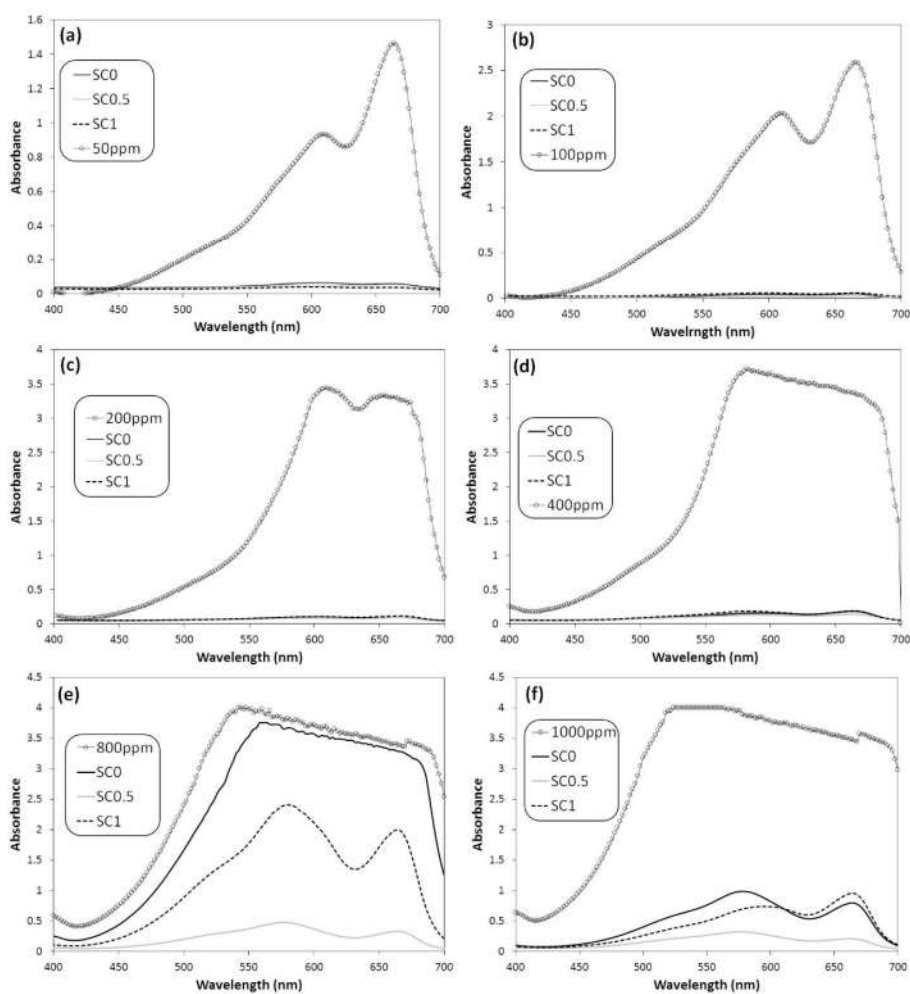


Fig. 6. UV-vis adsorption spectra of the aqueous MB solution in the presence of 3 mg of SC0, SC0.5 and SC1 samples at different MB concentrations, compared to the UV-vis spectrum of the MB solution without adding silica.

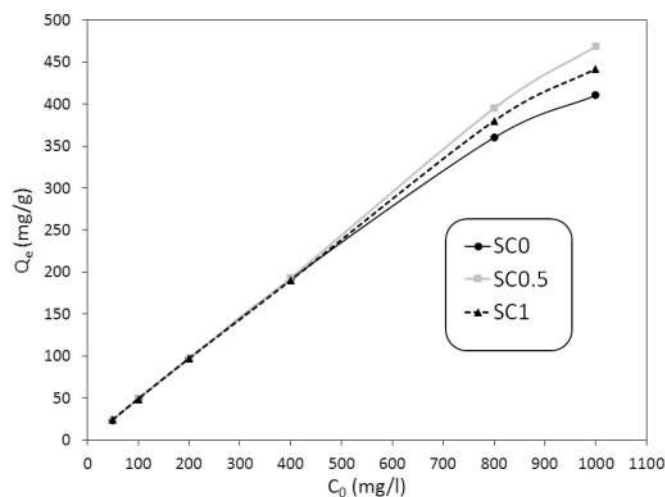


Fig. 7. Adsorption isotherms of MB on the SC0, SC0.5 and SC1.

The efficiencies of the synthesized mesoporous samples for MB removal from an aqueous solution are shown in Fig. 5. The MB initial concentration was 100 ppm. It can be observed that for all samples, the MB concentration in the solution after 2.5 min exposure of the contaminated solution to mesoporous silica powder reached to below 5 ppm and after that, the curve became nearly flat up to 20 min. Consequently, 20 min of exposure seems to be adequate time for the adsorption process which ensures the equilibrium concentration of MB in the solution to reach a steady state.

Fig. 6 shows the adsorption behavior of SC0, SC0.5 and SC1 samples after 20 min for the different MB concentrations in the corresponding aqueous solutions. For sake of comparison, the adsorption curves for MB solution without adding mesoporous silica were included in each part of the figure. It is clear that up to 400 ppm, SC0, SC0.5 and SC1 samples adsorbed almost the whole of MB in the solution. For higher concentrations, a small deviation was detected in the adsorption behavior of the samples. For MB concentrations greater than 400 ppm, SC0.5 sample unexpectedly showed the best adsorption result. More efficient adsorption behavior of SC0.5 sample than SC0 one is obviously reasonable due to its larger surface area, average

pore diameter, and also pore volume. Better adsorption behavior of SC0.5 sample than that of SC1, despite its lower surface area, may be attributed to its larger average pore diameter and pore volume than those in SC1. It seems that the average pore size of SC1 sample (4.1 nm, see Table 1) is too small for efficiently removing high concentrations of MB contamination from water in reasonably short times.

Using both curves depicted in Fig. 6 and Equation 1, the equilibrium adsorption capacities ( $Q_e$ ) of SC0, SC0.5 and SC1 samples were obtained, as shown in Fig. 7. As seen, SC0.5 sample has the greatest adsorption capacity among others. Using Equation 2, the maximum adsorption capacities ( $Q_m$ ) of SC0, SC0.5 and SC1 samples were calculated to be approximately 333, 454, and 526 mg/g, respectively.

#### 4. CONCLUSION

Mesoporous silica were synthesized via a sol-gel method in the acidic media using the CTAB as the structural directing agent. It was found that as the surfactant amount increased up to 1 g, the specific surface area increased up to 548.8  $\text{m}^2\cdot\text{g}^{-1}$ . Also, increasing the CTAB amount caused the pore volume to initially increase from about 1 to 2  $\text{cm}^3/\text{g}$ , which followed by a decrease to  $\sim 0.5$   $\text{cm}^3/\text{g}$ . The largest surface area and the lowest

pore volume were obtained in case of sample SC1. It was found that below MB concentration of 400 ppm, all synthesized samples have almost similar adsorption behavior, while for higher concentrations, small deviations were detected in removing MB contamination and SC0.5 sample exhibited a better adsorption.

## REFERENCES

1. Xu, R., Pang, W., Yu, J., Hou, Q. and Chen, J., "Chemistry of zeolites and related porous materials: synthesis and structure", John Wiley & Sons Inc, New Jersey, USA, 2007.
2. Barrabino, A., "Synthesis of mesoporous silica particles with control of both pore diameter and particle size". J. Bioeng. Biomed. Sci., MSc thesis, Department of chemical and biological technology, Chalmers University of Technology, Sweden, 2011.
3. Galan-Fereres, M., Alemany, L. J., Mariscal, R., Banares, M. A., Anderson, J. A. and Fierro, J. L. G., "Surface acidity and properties of titania-silica catalysts". Chem. Mater., 1995, 7, 1342–1348.
4. Hertz, A., FitzGerald, V., Pignotti, E., Knowles, J. C., Sen, T. and Bruce, I. J., "Preparation and characterisation of porous silica and silica/titania monoliths for potential use in bone replacement". Microporous Mesoporous Mater., 2012, 156, 51–61.
5. Smith, G. M., "Enzyme immobilisation and catalysis in ordered mesoporous silica". PhD thesis, School of chemistry, University of St. Andrews, Scotland, 2008.
6. Treccani, L., Klein, T. Y., Meder, F., Pardun, K. and Rezwan, K., "Functionalized ceramics for biomedical, biotechnological and environmental applications". Acta Biomater., 2013, 9, 170–223.
7. Meynen, V., Cool, P. and Vansant E. F., "Verified syntheses of mesoporous materials". Microporous Mesoporous Mater., 2009, 125, 170–223.
8. Johansson, E. M., "Controlling the pore size and morphology of mesoporous silica". BSc thesis, Department of physics, chemistry and biology, Linköping University, Sweden, 2010.
9. Shibata, H., Mihara, H., Mukai, T., Ogura, T., Kohno, H., Ohkubo, T., Sakai, H. and Abe, M., "Preparation and formation mechanism of mesoporous titania particles having crystalline wall". Chem. Mater., 2006, 18, 2256–2260.
10. Bielawska, M., Chodzińska, A., Jańczuk, B. and Zdziennicka, A., "Determination of CTAB CMC in mixed water+ short-chain alcohol solvent by surface tension". Colloids Surf., A, 2013, 424, 81–88.
11. Lee, Y. S., Jang, W., Koo, H. Y. and Choi, W. S., "Facile synthesis of mesoporous SiO<sub>2</sub> nanoparticles using the mobility differences of etchants". RSC Adv., 2015, 5, 26223–26230.
12. Zhu, M. Lee, L., Wang, H. and Wang Z., "Removal of an anionic dye by adsorption/precipitation processes using alkaline white mud". J. Hazard. Mater., 2007, 149, 735–741.
13. Jiao, Y., Guo, J., Shen, S., Chang, B., Zhang Y., Jiang, X. and Yang, W., "Synthesis of discrete and dispersible hollow mesoporous silica nanoparticles with tailored shell thickness for controlled drug release". J. Mater. Chem., 2012, 22, 17636–17643.
14. Zhu, A., Shi, J., Chen, H., Shen, W. and Dong, X., "A facile method to synthesize novel hollow mesoporous silica spheres and advanced storage property". Microporous Mesoporous Mater., 2005, 84, 218–222.
15. Pavan, F. A., Mazzocato, A. C. and Gushikem Y., "Removal of methylene blue dye from aqueous solutions by adsorption using yellow passion fruit peel as adsorbent". Bioresour. Technol., 2008, 99, 3162–3165.
16. Ponnusami, V., Madhuran, R., Krithika, V. and Srivastava, S. N., "Effects of process variables on kinetics of methylene blue sorption onto untreated guava (Psidium guajava) leaf powder: Statistical analysis". Chem. Eng. J., 2008, 140, 609–613.
17. Whang, T. J., Hsieh, M. T. and Chen, H. H., "Visible-light photocatalytic degradation of methylene blue with laser-induced Ag/ZnO nanoparticles". Appl. Surf. Sci., 2012, 258, 2796–2801.
18. Zhao, X. S., Lu, G. Q. and Millar, G. J., "Advances in mesoporous molecular sieve MCM-41". Ind. Eng. Chem. Res., 1996, 35, 2075–2090.

19. Somasiri, W., Li, X. F., Ruan, W. Q. and Jian C., "Evaluation of the efficacy of upflow anaerobic sludge blanket reactor in removal of colour and reduction of COD in real textile wastewater". *Bioresour. Technol.*, 2008, 99, 3692–3699.
20. Aksu, Z., "Application of biosorption for the removal of organic pollutants: a review". *Process Biochem.*, 2005, 40, 997–1026.
21. Ho, Y. S., Malarvizhi, R. and Sulochana, N., "Equilibrium isotherm studies of methylene blue adsorption onto activated carbon prepared from *Delonix regia* pods". *J. Environ. Prot. Sci.*, 2009, 3, 111–116.
22. Yang, L., Sheldon, B. W. and Webster, T. J., "Nanophase ceramics for improved drug delivery: current opportunities and challenges". *Am. Ceram. Soc. Bull.*, 2010, 89, 24–32.
23. Fan, Z. J., Kai, W., Yan, J., Wei, T., Zhi, L. J., Feng, J., Ren, Y., Song, L. P. and Wei F., "Facile synthesis of graphene nanosheets via Fe reduction of exfoliated graphite oxide". *ACS Nano*, 2010, 5, 191–198.
24. Maleki, M., Beitollahi, A., Javadpour, J. and Yahya, N., "Dual template route for the synthesis of hierarchical porous boron nitride". *Ceram. Int.*, 2015, 41, 3806–3813.
25. Wang, M., Xia, Y., Wang, X., Xiao, Y., Liu, R., Wu, Q., Qiu, B., Metwalli, E., Xia, S. and Yao Y., "SiOC/Carbon Nanohybrids with Tiny SiOC Particles Embedded in Free Carbon Matrix Based on Photoactive Dental Methacrylates". *ACS Appl. Mater. Interfaces*, 2016, 8, 13982–13992.
26. Kleitz, F., "Ordered mesoporous materials: template removal, frameworks and morphology". PhD thesis, Faculty of Chemistry, The Ruhr-University Bochum, 2002.
27. Zheng, H. and Che, S., "Amino/quaternary ammonium groups bifunctionalized large pore mesoporous silica for pH-responsive large drug delivery". *RSC Adv.*, 2012, 2, 4421–4429.
28. Hilonga, A., Kim, J. K., Sarawade, P. B. and Kim, H. T., "Mesoporous titania–silica composite from sodium silicate and titanium oxychloride, Part II: one-pot co-condensation method". *J. Mater. Sci.*, 2010, 45, 1264–1271.